Supplementary Material for:

ESR-thermochronometry of the MIZ1 borehole, Tono, Japan

G.E. King[1]*, L. Bossin[1,2], M. Bernard[1], M. Kranz-Bartz[1,3], X. Wen[1], C. Schmidt[1], F. Herman[1], M. Ogata[4], S. Sueoka[4]

[1]Institute of Earth Surface Dynamics, University of Lausanne, Switzerland.
[2]Paul Scherrer Institute, Villigen, Switzerland.
[3]Institute of Geosciences, Ruhr-University Bochum, Germany.
[4]Tono Geoscience Center, Japan Atomic Energy Agency, Toki, Japan.

Correspondence to: Georgina E. King (georgina.king@unil.ch)

All data and the codes used in this study are available for download here: https://tinyurl.com/2rmfwkv7 (to update following manuscript acceptance)

Table S1: Equivalent dose and *n*/*N* values for the different samples and centres. D_e values calculated from sample specific dose response curves and the standardised dose response curve using different fitting options are listed.

Table S2: Sample and centre specific kinetic parameters.

Table S3: Data input and output from DRAC v.1.2 (Durcan et al., 2015) for calculation of the environmental dose rate.

Table S4: Dose recovery test results

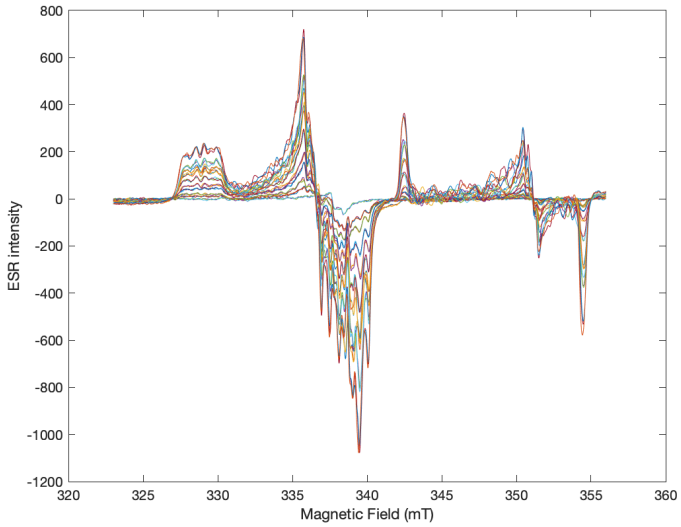

Figure. S1: Measured ESR spectra of sample MIZ1-05 (aliquot A), following different regenerative doses. This sample is representative of the investigated samples.

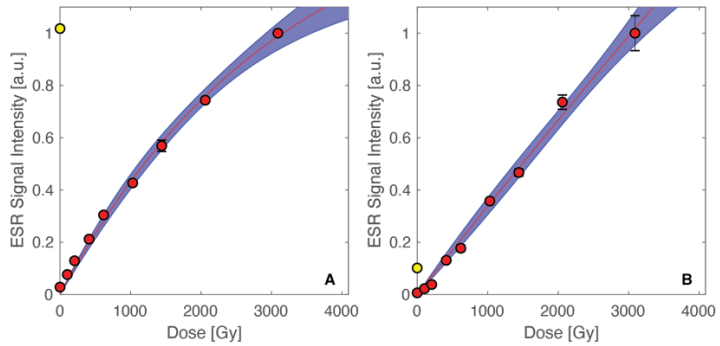

Figure S2: Individual SAR dose response of (A) the Al-centre and (B) Ti-centre option D for sample MIZ1-01 fitted with an SSE function (red line). The 1σ error range is shown in blue. Yellow data points are the natural signal intensity and red data points are laboratory regenerative irradiations. Note the sub-linearity in dose response for the Ti-centre.

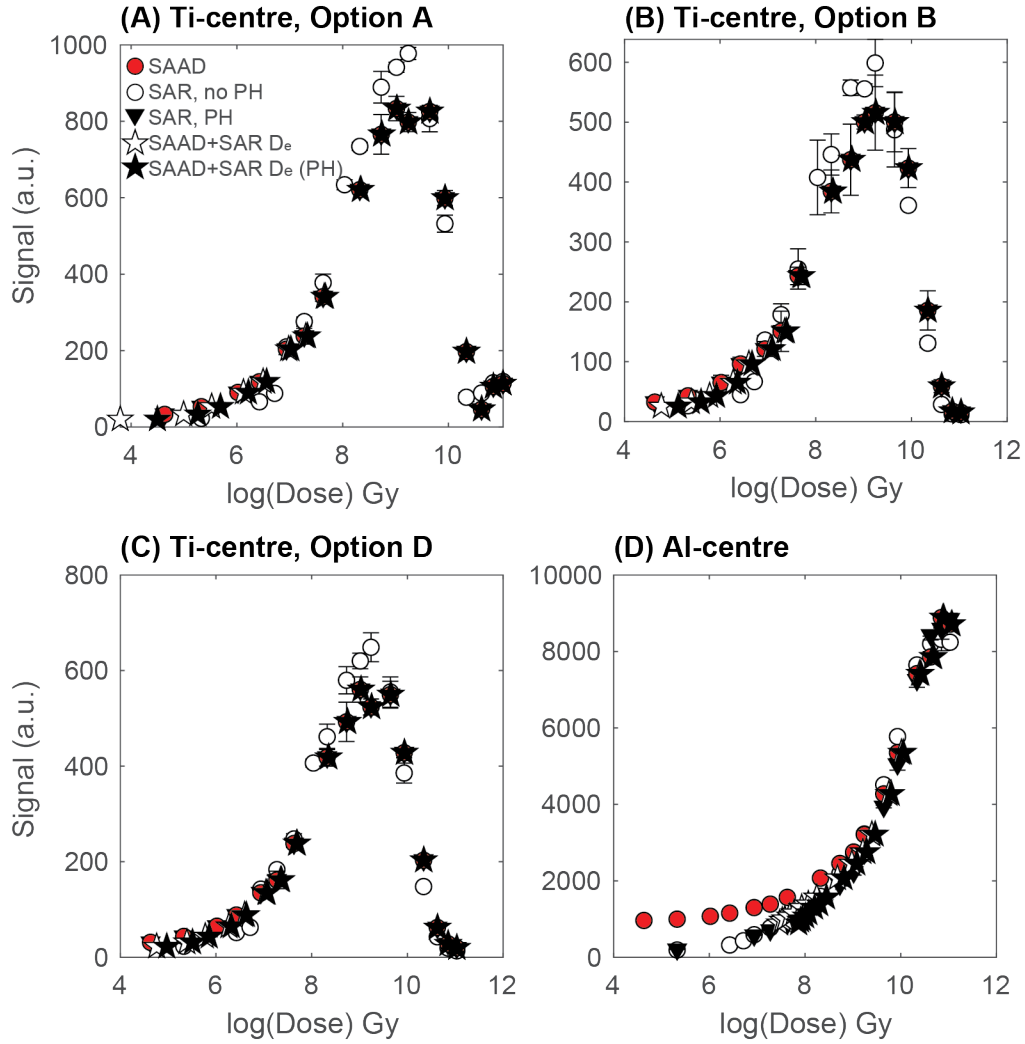

Figure S3: Comparison between SAR and SAAD dose response curves measured for different aliquots of sample MIZ1-08.

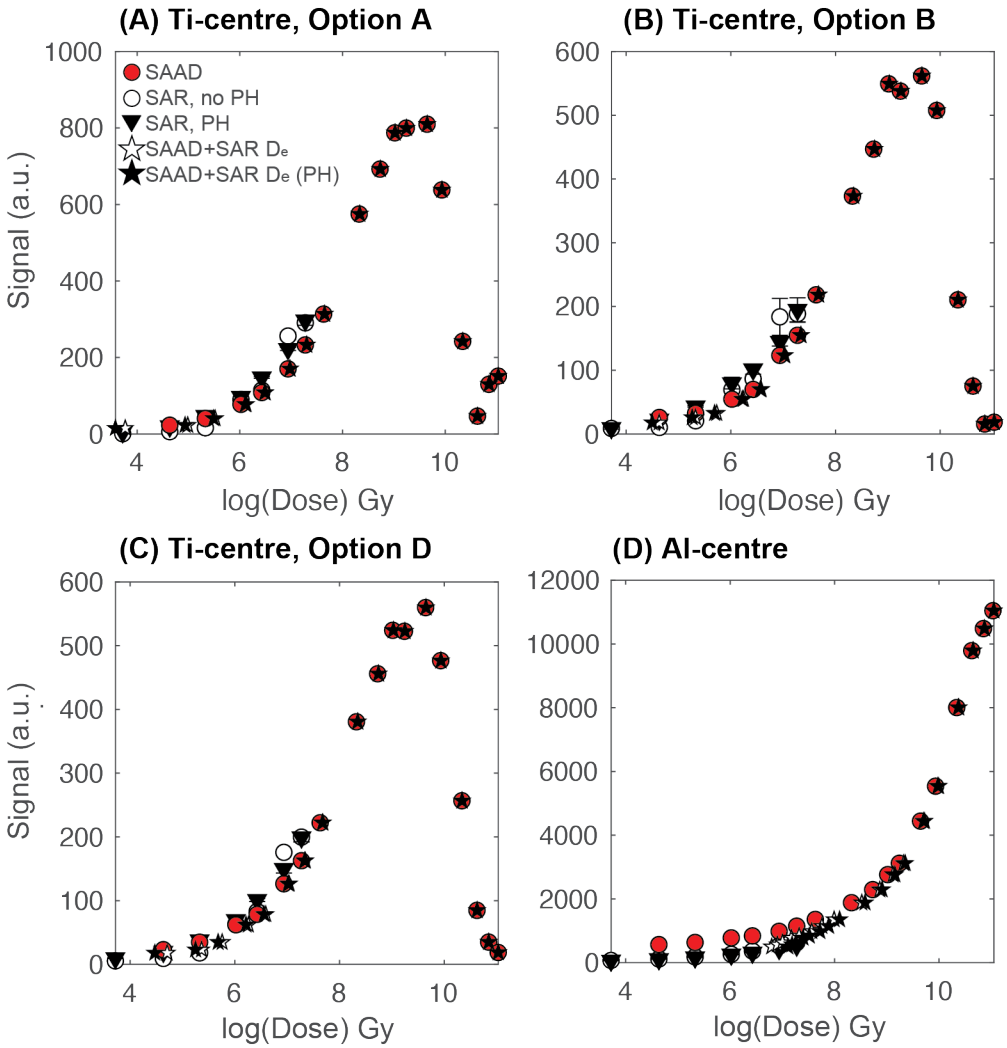

Figure S4: Comparison between SAR and SAAD dose response curves measured for different aliquots of sample MIZ-1-10.

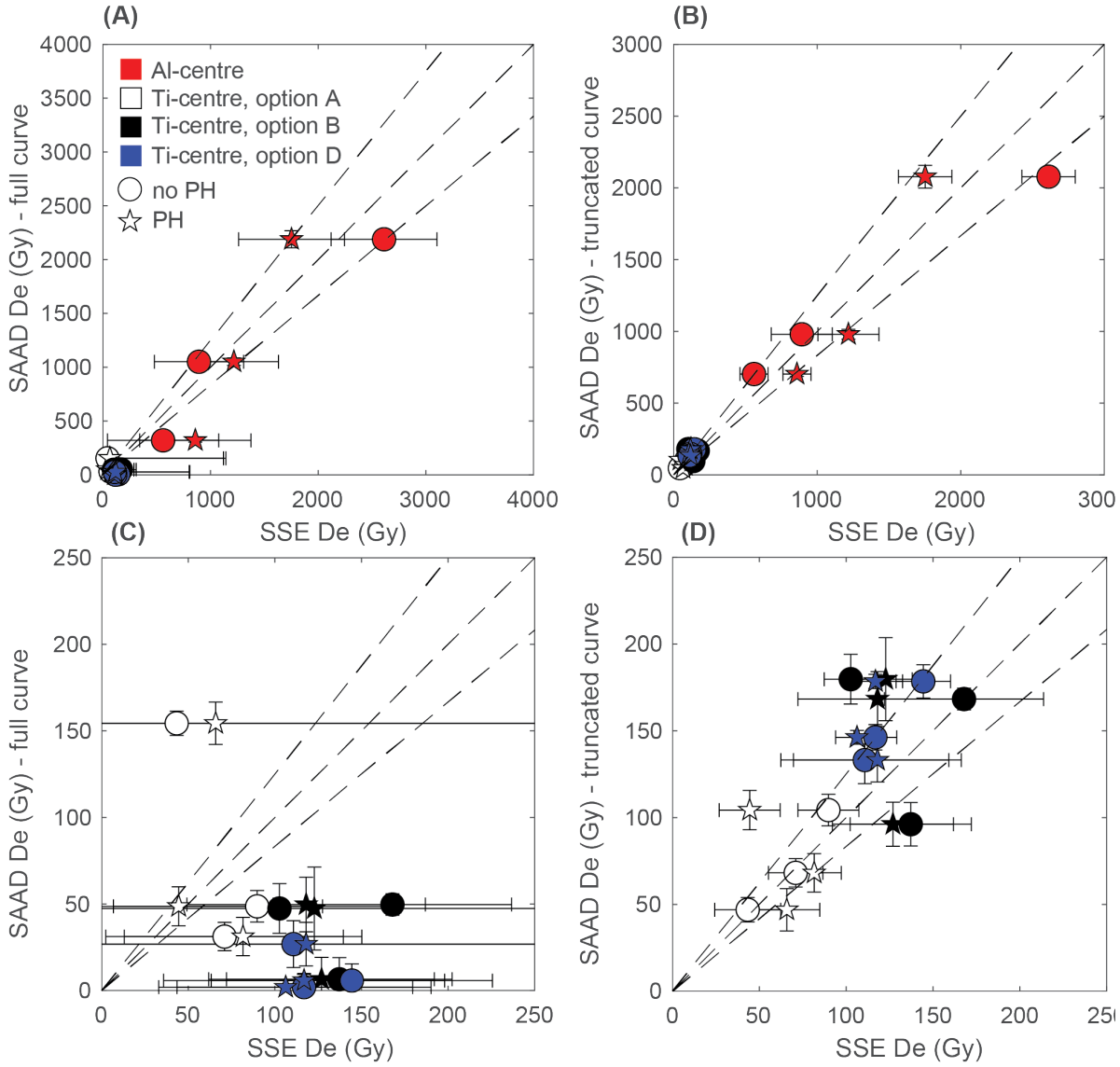

Figure S5: Deviation between SAR and SAAD derived equivalent dose (D_e) values for the Al- and Ti centres of samples MIZ1-08, MIZ1-09 and MIZ1-10. (A) and (C) individual SAR SSE D_e values in comparison to SAAD D_e values interpolated from the complete SAAD DRC (i.e. dosed into saturation), and (B) and (D) interpolated onto the SAAD DRC truncated at 4.5 kGy (see discussion in main text). Some aliquots measured for SAR were not preheated (circles), all SAAD measurements were preheated – see discussion in main text.

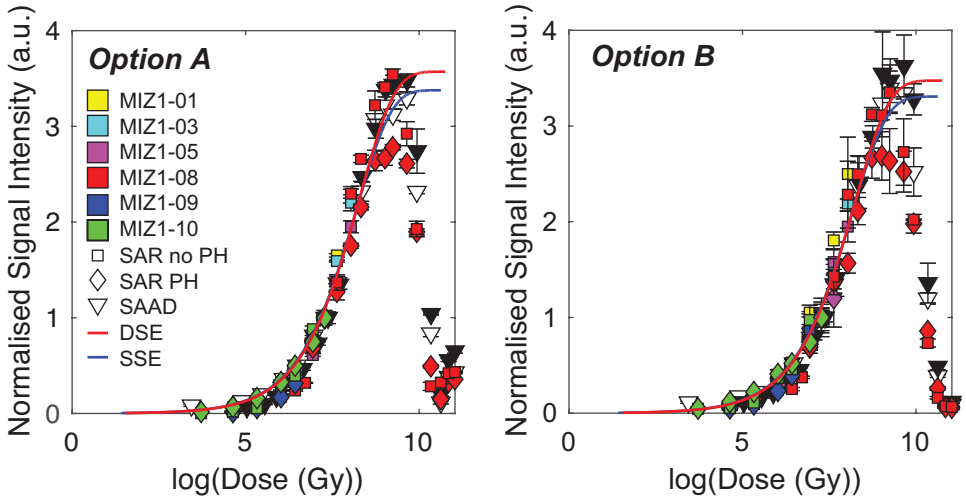

Figure S6: SAAD and SAR data for all samples, normalised by an arbitrary dose of 1,442 Gy for the Ti-centre Option A and Option B. Standardised growth curve data fits are shown.

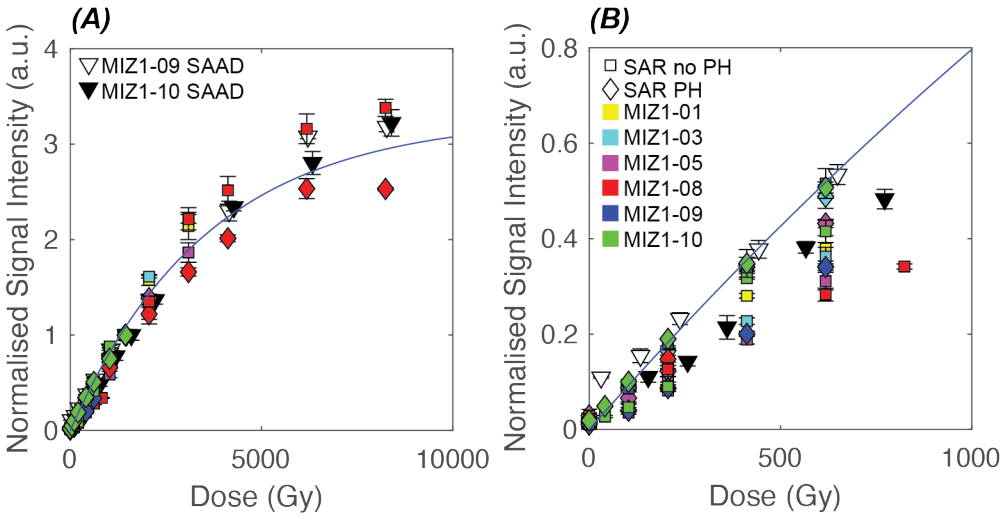

Figure S7: SAAD and SAR data for all samples, normalised by an arbitrary dose of 1,442 Gy for the Ti-centre Option D. The data are fitted with an SSE function and are not plotted in log space to allow the deviation between the measured data and the modelled fit to be visible. Note that the complete dataset has been fitted, but the figures are truncated to allow the lower part of the dose response curve to be visualised. (A) Dose response plotted up to 10 kGy, (B) plotted up to 1 kGy.

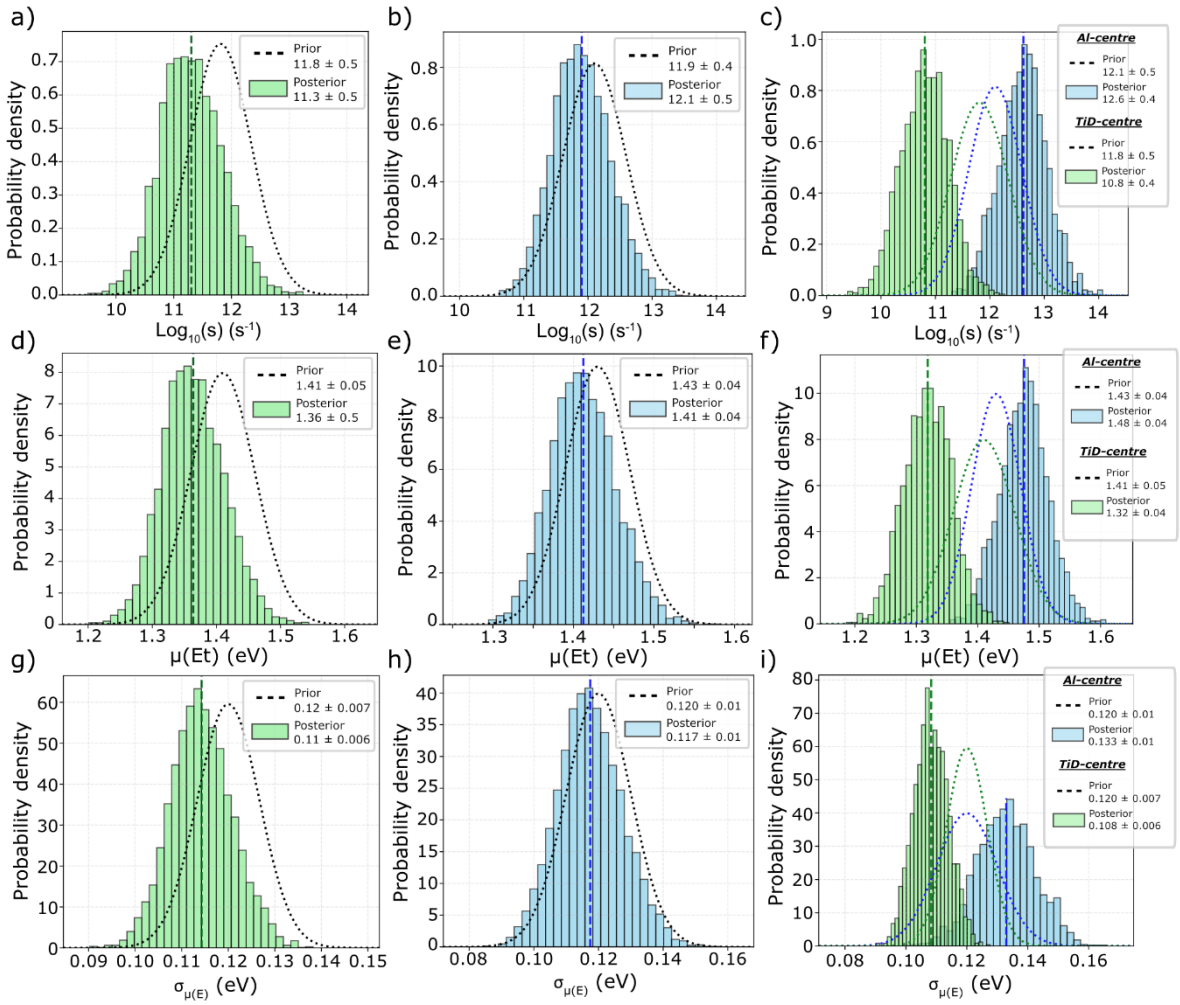

Figure S8. Sampling distribution of kinetic parameter values from vertical profile inversions. Sampling distributions are shown for (a-c) the frequency factor (s, Table 1), (d-f) the mean trap depth (μ(Et), Table 1), and (g-i), the standard deviation of trap depth ($\sigma_{\mu(Et)}$, Table 1).

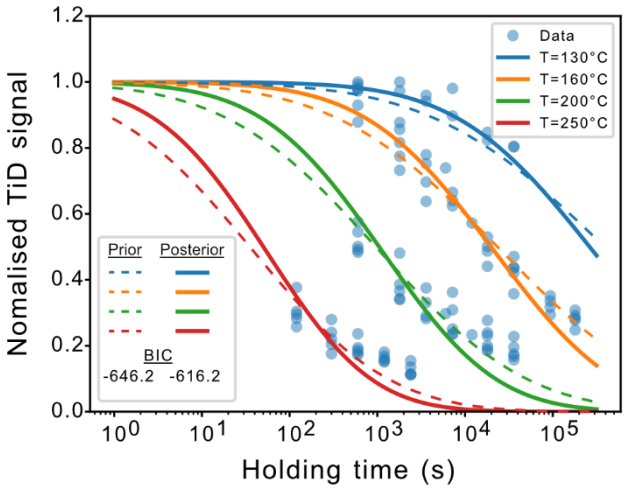

Figure S9. Fit to isothermal experiments data for the TiD centre. The model fits are shown for the prior kinetics (solid lines) extracted by fitting laboratory data (blue circles) and for the posterior kinetic (dashed lines) extracted from the vertical profile inversions (see Fig. S9).

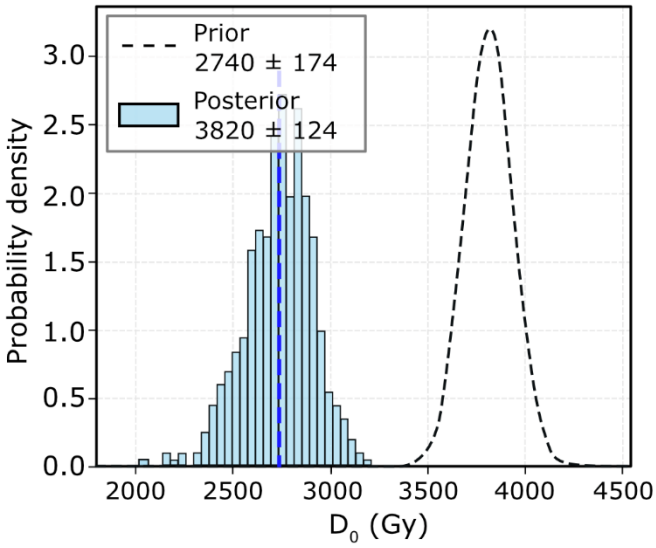

Figure S10. Sampling distribution of D0 values from vertical profile inversion. Additional inversion is run by fixing temperature histories of all samples at borehole temperature for 30 Myr and prior thermal kinetic parameters. Only D0 and n/N values are allowed to vary according to their correlation. The prior and the posterior distributions are shown (see main text for discussion).

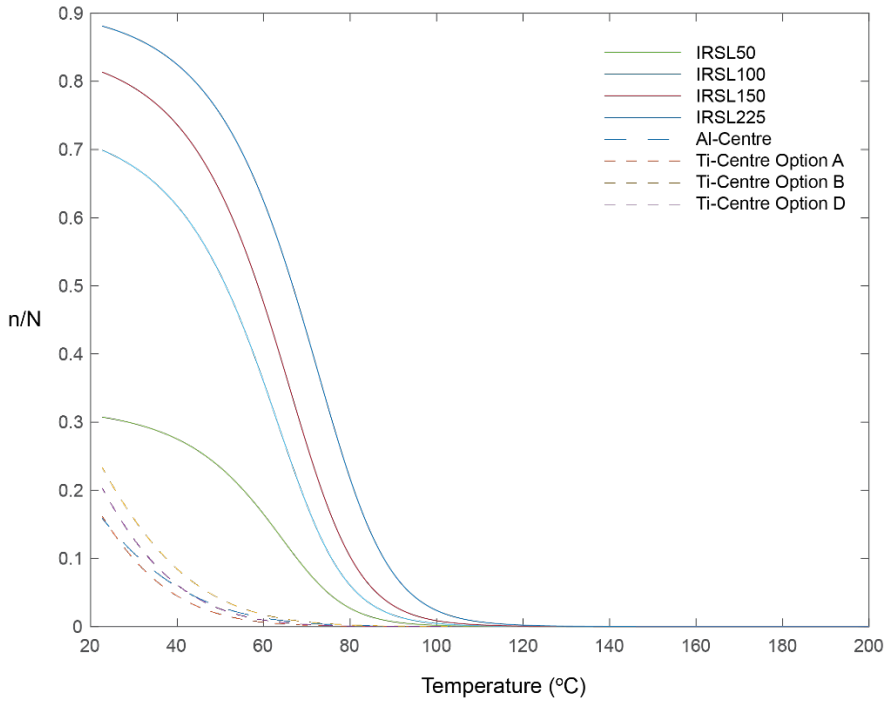

Figure S11: Forward modelling of the OSL and ESR data of sample MIZ1-01. OSL data taken from Ogata et al. (2022), ESR data taken from this study. A forward model was run assuming monotonic cooling from 200 °C to the modern-day ambient borehole temperature of 22.7 °C over 40 Ma. Whilst the cooling history is unrealistic for these samples, given the constraint of the AFT ages that indicate a maximum temperature of ~60 °C, 40 Ma ago, it allows us to see the different closure temperatures of the different systems. The OSL data were modelled in the same way as in Ogata et al. (2011), i.e. using the approach of King et al. (2016) whereby the band-tail states model (Li and Li, 2013) is used to describe thermal decay, a single saturating exponential fit is used to describe dose response and athermal decay is described following Huntley (2006). The ESR data were modelled following the approach of King et al. (2020) whereby the Gauss model is used to describe thermal decay (Lambert, 2018) and dose response is described using a single saturating exponential function.

References

Durcan, J.A., King, G.E. and Duller, G.A.: DRAC: Dose Rate and Age Calculator for trapped charge dating. *Quaternary Geochronology*, *28*, pp.54-61, 2015.

Huntley, D.J.: An explanation of the power-law decay of luminescence. *Journal of Physics: Condensed Matter*, *18*(4), p.1359, 2006.

King, G.E., Herman, F., Lambert, R., Valla, P.G. and Guralnik, B.: Multi-OSL-thermochronometry of feldspar. *Quaternary Geochronology*, *33*, pp.76-87, 2016.

King, G.E., Tsukamoto, S., Herman, F., Biswas, R.H., Sueoka, S. and Tagami, T.: Electron spin resonance (ESR) thermochronometry of the Hida range of the Japanese Alps: validation and future potential. *Geochronology*, *2*(1), pp.1-15, 2020.

Lambert, R.: Investigating thermal decay in K-feldspar for the application of IRSL thermochronometry on the Mont Blanc massif, Unpublished PhD Thesis, University of Lausanne, Switzerland, 2018.

Li, B. and Li, S.H.: The effect of band-tail states on the thermal stability of the infrared stimulated luminescence from K-feldspar. *Journal of Luminescence*, *136*, pp.5-10, 2013.

Ogata, M., King, G.E., Herman, F. and Sueoka, S.: Reconstructing the thermal structure of shallow crust in the Tono region using multi-OSL-thermometry of K-feldspar from deep borehole core. *Earth and Planetary Science Letters*, *591*, p.117607, 2022.